Observation of Dicke cooperativity in magnetic interactions

Article *in* Science · August 2018

DOI: 10.1126/science.aat5162

CITATIONS
23

READS
1,087

13 authors, including:

Xinwei Li
California Institute of Technology
38 PUBLICATIONS **322** CITATIONS
SEE PROFILE

Motoaki Bamba
Osaka University & PRESTO (JST)
55 PUBLICATIONS **724** CITATIONS
SEE PROFILE

Ning Yuan
Shanghai University
7 PUBLICATIONS **31** CITATIONS
SEE PROFILE

Qi Zhang
Nanjing University
59 PUBLICATIONS **1,530** CITATIONS
SEE PROFILE

MAGNETISM

Observation of Dicke cooperativity in magnetic interactions

Xinwei Li[1], Motoaki Bamba[2,3], Ning Yuan[4], Qi Zhang[5], Yage Zhao[6], Maolin Xiang[4], Kai Xu[4], Zuanming Jin[4], Wei Ren[4], Guohong Ma[4], Shixun Cao[4]*, Dmitry Turchinovich[7,8], Junichiro Kono[1,9,10]*

The interaction of *N* two-level atoms with a single-mode light field is an extensively studied many-body problem in quantum optics, first analyzed by Dicke in the context of superradiance. A characteristic of such systems is the cooperative enhancement of the coupling strength by a factor of $\sqrt{N}$. In this study, we extended this cooperatively enhanced coupling to a solid-state system, demonstrating that it also occurs in a magnetic solid in the form of matter-matter interaction. Specifically, the exchange interaction of *N* paramagnetic erbium(III) (Er^{3+}) spins with an iron(III) (Fe^{3+}) magnon field in erbium orthoferrite ($ErFeO_3$) exhibits a vacuum Rabi splitting whose magnitude is proportional to $\sqrt{N}$. Our results provide a route for understanding, controlling, and predicting novel phases of condensed matter using concepts and tools available in quantum optics.

When an ensemble of two-level atoms interacts with a single-mode long-wavelength light field, coherence can develop within the ensemble through photon exchange; the interaction becomes cooperative. This phenomenon, captured by the Dicke superradiance model (*1*), has profound consequences in cavity quantum electrodynamics (QED) research. In a photonic cavity, the coupling rate Λ between N dipoles and a quantized vacuum photon field is cooperatively enhanced by a factor of $\sqrt{N}$ (*2*). The ground state of the atom ensemble is predicted to be unstable against a phase transition, known as the superradiant phase transition (SRPT), when Λ reaches a critical value (*3*). This possibility has stimulated much recent interest in condensed matter cavity QED systems consisting of N dipoles with very large moments (*4*–*7*).

The role light plays in the Dicke model can be performed by any fundamental excitation—such as lattice waves (phonons) and spin waves (magnons)—that can be bosonized and quantized in the same way as photons. This concept of Dicke physics without light is crucial for understanding phase transitions in condensed matter. The most relevant example is the cooperative Jahn-Teller (JT) effect, which describes the dynamics of an ensemble of pseudospins with degenerate electronic levels cooperatively coupled with a phonon mode in the same material. The cooperative coupling leads to a phase transition that distorts the lattice and breaks the degeneracy of the pseudospin energy levels. Theoretically, the transition is believed to be analogous to the SRPT (*8*); the displacive lattice distortion is comparable to the appearance of a static electromagnetic field in the photon SRPT. Although these theories can explain JT and JT-like transitions phenomenologically, unambiguous evidence for the cooperative coupling of two matter subsystems in one material system is still lacking.

Here we report cooperative exchange coupling of a spin ensemble with a vacuum magnon field within a solid. We used Y^{3+}-doped single-crystal $ErFeO_3$ samples—namely, $Er_xY_{1-x}FeO_3$—and systematically studied the doping, temperature, and magnetic field dependence of their terahertz (THz) absorption spectra. The Er^{3+} electron paramagnetic resonance (EPR) in an external magnetic field strongly coupled with a vacuum magnon mode of the ordered Fe^{3+} spins. The situation is analogous to a standard N-atom cavity QED experiment, in which an ensemble of N two-level atoms couples with a vacuum photon field in an optical cavity. The Fe^{3+}-Er^{3+} coupling rate showed a characteristic scaling behavior with the density of Er^{3+} ions, evidencing Dicke cooperativity. By analyzing this scaling behavior with our microscopic theoretical model, we determined the Fe^{3+}-Er^{3+} exchange coupling constants. These constants are important for understanding the widely discussed 3d-4f magnetic coupling that is responsible for many exotic phenomena in a variety of compounds: examples include novel magnetic phase transitions (*9*), magnetoelectric effects (*10*, *11*), electromagnons (*12*), nonlinear spin excitations (*13*), and heavy fermions (*14*).

$ErFeO_3$ crystallizes in an orthorhombic perovskite structure (Fig. 1A) that can be described by the space group D_{2h}^{16}-*Pbnm*. The Fe^{3+} spins order antiferromagnetically below 650 K. Many magnetic phases—such as the Γ_4, Γ_{24}, Γ_2, and Γ_{12} phases—can appear as a function of temperature (*15*). In the temperature range 4.5 K < T < 85 K, the crystal is in the Γ_2 phase, in which the spins in the two Fe^{3+} sublattices, $\mathbf{S}_1$ and $\mathbf{S}_2$, are antiparallel along the c axis but cant toward the a axis by a small angle β, owing to the antisymmetric Dzyaloshinskii-Moriya interaction (Fig. 1, A and B). The sum of the two spins $\mathbf{S}_+ = \mathbf{S}_1 + \mathbf{S}_2$ induces $\mathbf{M}_{Fe} \| a$, where $\mathbf{M}_{Fe}$ is the macroscopic magnetization vector of the Fe^{3+} subsystem. The quasi-ferromagnetic (qFM) magnon mode of the Fe^{3+} subsystem can be selectively excited by using linearly polarized THz radiation with $\mathbf{H}_{THz} \perp a$ (*16*, *17*), where $\mathbf{H}_{THz}$ is the magnetic component of the THz electromagnetic field. Figure 1B shows how the Fe^{3+} spins oscillate in the qFM mode. $\mathbf{S}_1$ and $\mathbf{S}_2$ oscillate in phase while the angle between them remains constant, so the model can be reduced to the precession of the combined spin $\mathbf{S}_+$ about the a axis.

On the other hand, the Er^{3+} ions ($4f^{11}$) occupy low-symmetry sites in the crystal. The crystal field forms Kramers doublets; each doublet

[1]Department of Electrical and Computer Engineering, Rice University, Houston, TX 77005, USA. [2]Department of Materials Engineering Science, Osaka University, Osaka 560-8531, Japan. [3]PRESTO, Japan Science and Technology Agency, Saitama 332-0012, Japan. [4]Department of Physics, International Center of Quantum and Molecular Structures, and Materials Genome Institute, Shanghai University, Shanghai 200444, China. [5]Argonne National Laboratories, Lemont, IL 60439, USA. [6]School of Physics, Peking University, Beijing 100871, China. [7]Fakultät für Physik, Universität Duisburg-Essen, Lotharstr. 1, Duisburg 47057, Germany. [8]Max Planck Institute for Polymer Research, Ackermannweg 10, Mainz 55128, Germany. [9]Department of Materials Science and NanoEngineering, Rice University, Houston, TX 77005, USA. [10]Department of Physics and Astronomy, Rice University, Houston, TX 77005, USA.
*Corresponding author. Email: kono@rice.edu (J.K.); sxcao@shu.edu.cn (S.C.)

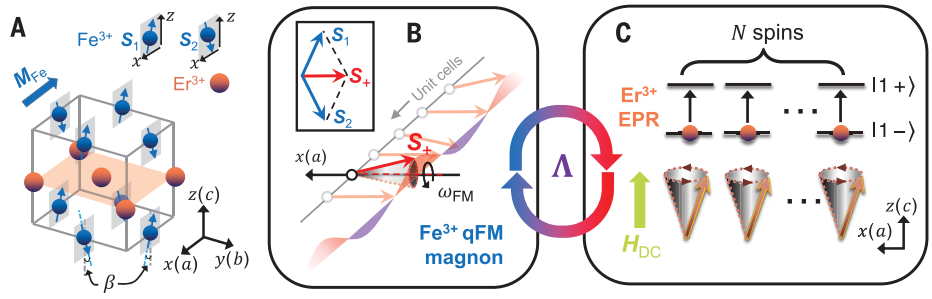

Fig. 1. Cooperatively coupled *N*-spin–magnon system as an analog of an *N*-atom cavity QED system. (**A**) Crystal and magnetic structure of $ErFeO_3$ in the Γ_2 phase. (**B**) Oscillations of spins in the qFM magnon mode of the Fe^{3+} subsystem in the Γ_2 phase. (**C**) The EPR of the Er^{3+} spin ensemble is the transition between the lowest Kramers-doublet states. The two matter subsystems, illustrated in (B) and (C), are resonantly coupled with the coupling constant Λ.

consists of a pair of time-reversed states. As shown in Fig. 1C, when an external static magnetic field ($\mathbf{H}_{DC}$) is applied, and in the low-temperature limit, the transition between the lowest two time-reversed states ($|1-\rangle$ and $|1+\rangle$) can be interpreted as the EPR of the ion. In a classical picture, the EPR corresponds to the Larmor precession of spins about $\mathbf{H}_{DC}$. The N Er^{3+} spins within a characteristic volume interact cooperatively with the Fe^{3+} qFM magnon mode at rate Λ. The rate can be determined by mapping out anticrossings through THz magnetospectroscopy.

Figure 2A shows the THz absorption spectra obtained from a c-cut $ErFeO_3$ single crystal; the measurement configuration was $\mathbf{H}_{THz} \| b$ and $\mathbf{H}_{DC} \| c$, and the temperature was 45 K (the crystal was in the Γ_2 phase, both in this experiment and the ones described hereafter). On the basis of a comprehensive series of complementary measurements and theoretical analyses (*18*), we assigned the constant-frequency line to be the Fe^{3+} qFM magnon mode and the line that increases linearly with $\mathbf{H}_{DC}$ to be the Er^{3+} EPR mode.

We observed a clear temperature-dependent magnon-EPR anticrossing behavior (Fig. 2, B to E). The zero-detuning magnetic field, H_0, is the magnitude of $\mathbf{H}_{DC}$ at which the uncoupled magnon and EPR mode frequencies are equal; this frequency is the zero-detuning transition frequency, ω_0. Experimentally, H_0 also coincides with the magnitude of $\mathbf{H}_{DC}$ at which the frequency difference between the hybridized branches reaches a minimum. The frequency splitting between the hybridized branches at H_0, which we call the vacuum Rabi splitting $\Omega(H_0)$, is equal to twice the magnon-EPR coupling strength Λ. The magnitude of Λ increases with decreasing temperature, indicating that the Fe^{3+}-Er^{3+} coupling becomes stronger.

Here we provide some interpretations to several features in the data. First, there is some fine structure in the middle of the anticrossing region. This can be modeled by considering two species of Er^{3+} ions (due to the $\mathbf{H}_{DC}$-induced sublattice degeneracy breaking) interacting with the Fe^{3+} magnons; however, the feature can be neglected if we effectively consider the two Er^{3+} species as one (*18*). Next, the intensity variations of the absorption lines are due to the $\mathbf{H}_{DC}$-induced mixing of crystal field levels. Finally, the magnon frequency bowing for the 5 K spectra is due to the spin structure instability, as the temperature is close to the critical point where a Γ_2-to-Γ_{12} spin reorientation transition occurs (*18*).

To determine how Λ grows with the Er^{3+} spin density, we studied Y^{3+}-doped $ErFeO_3$ single crystals ($Er_xY_{1-x}FeO_3$). It has been previously shown that the nonmagnetic Y^{3+} ions simply reduce the density of Er^{3+} spins by a factor of x without changing the crystal or magnetic structure of the system (*19*). In Fig. 2, panels F to H (and I to K, respectively) show temperature-dependent anticrossing spectra for the $x = 0.75$ ($x = 0.5$) sample. An increasing Λ at lower temperatures is again found. In addition, comparison among Fig. 2, C, F, and I, indicates that, at the same temperature

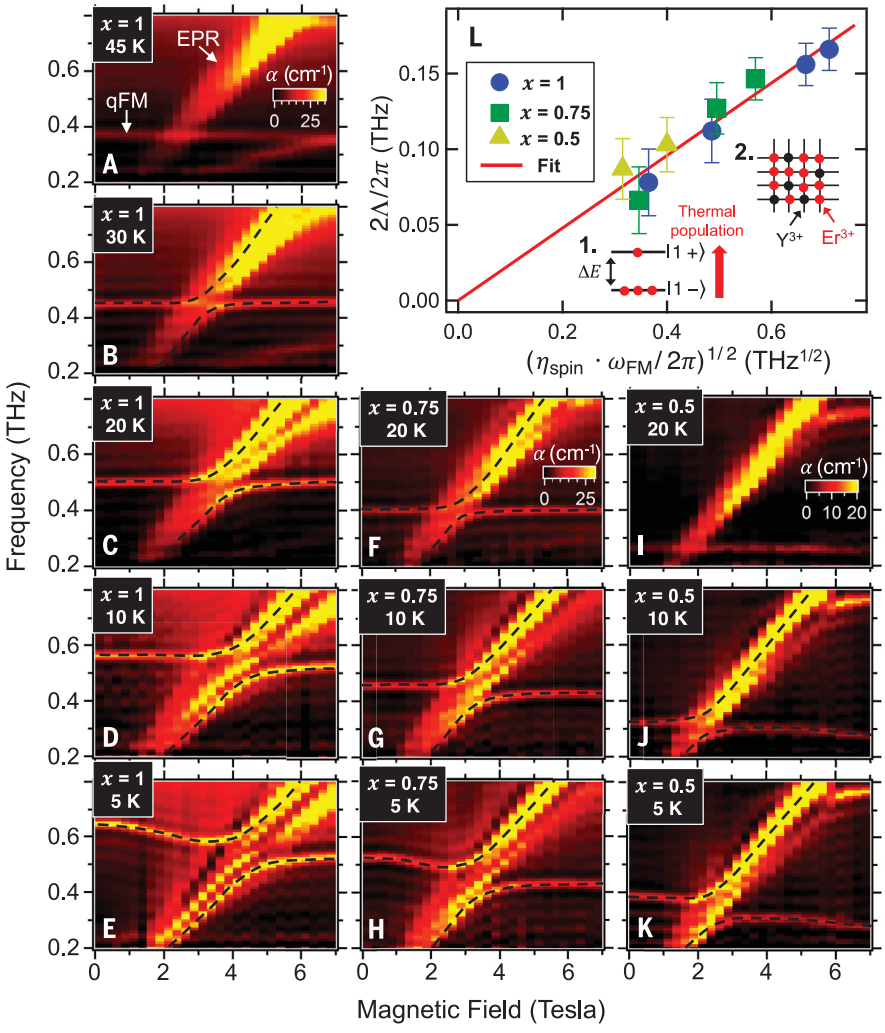

Fig. 2. Experimental evidence for cooperative coupling between paramagnetic Er^{3+} spins and Fe^{3+} vacuum magnons. (**A** to **K**) Absorption spectra measured in the $\mathbf{H}_{THz} \| b$ and $\mathbf{H}_{DC} \| c$ configurations at various temperatures and Y^{3+} doping levels. Dashed black lines are guides to the eye for identifying the hybridized modes. (**L**) The coupling rate Λ shows proportionality with $\sqrt{\eta_{spin}\omega_{FM}}$. Error bars indicate the uncertainties in determining mode frequencies due to finite mode linewidths. The inset shows two types of mechanisms that determine η_{spin} in the measurements shown in (A) to (K).

(20 K), a larger value of x leads to a larger Λ. The same trend can also be observed from the doping-dependent data at 10 K (Fig. 2, D, G, and J) and 5 K (Fig. 2, E, H, and K). Notably, the system exhibited the largest $\Lambda/\omega_0 = 0.18$ when $x = 0.5$ and $T = 5$ K (Fig. 2K); this puts the system into the ultrastrong coupling regime, defined by $\Lambda/\omega_0 > 0.1$ in the language of cavity QED (*20*, *21*). Most importantly, we found that $\Lambda \propto \sqrt{n_{spin}\omega_{FM}}$, where n_{spin} is the net density of EPR-contributing Er^{3+} spins (a function of T, H_0, and x) and ω_{FM} is the Fe^{3+} qFM magnon frequency. Below, we discuss the physical meaning of this scaling law in terms of Dicke cooperativity.

First, we can understand how n_{spin} varies with T, H_0, and x, as depicted in the inset to Fig. 2L. At low T, we can approximate the Er^{3+} ions to be two-level systems that obey the Boltzmann statistics (*22*). Calculating the populations of the spin-up ($|1+\rangle$) and spin-down ($|1-\rangle$) states at T leads to the Curie law, $\langle\mu_{Er}\rangle/\mu_{sat} = \tanh(-\Delta E(T,H_0)/2k_BT)$, where $\langle\mu_{Er}\rangle$ is the average Er^{3+} magnetic moment per spin; μ_{sat} is the Er^{3+} saturation moment per spin, corresponding to $T = 0$; $\Delta E(T, H_0)$ is the T- and H_0-dependent energy level separation between $|1+\rangle$ and $|1-\rangle$; and k_B is the Boltzmann constant. Hence, $\langle\mu_{Er}\rangle$ monotonically increases as T decreases. In addition, the doping by nonmagnetic Y^{3+} ions simply reduces the density of Er^{3+} spins by a factor of x through dilution. Combining these effects, we can express the net Er^{3+} spin density as $n_{spin}(T, H_0, x) = \eta_{spin} \cdot n^0_{spin}$, where $\eta_{spin} \equiv x \cdot \tanh(-\Delta E/2k_BT)$ is the net fraction of EPR-contributing spins and $n^0_{spin} \equiv 2/V_0$ is the total Er^{3+} spin density in $ErFeO_3$ with V_0 being the unit-cell volume.

Second, we explain why the Fe^{3+} qFM magnon frequency ω_{FM} appears in the scaling equation

of Λ. In a semiclassical description of two-level systems interacting with a cavity light field, a photonic mode frequency that is analogous to ω_{FM} here also emerges in the expression of the vacuum Rabi splitting. This is due to the fact that the vacuum Rabi splitting is proportional to the vacuum fluctuation field of a quantized boson mode, and the vacuum field amplitude itself is proportional to the square root of the boson mode frequency. In our case, the Fe^{3+} vacuum magnon field scales with $\sqrt{\omega_{FM}}$ and affects the hybrid Fe^{3+}-Er^{3+} mode frequency splitting. In our experiments, ω_{FM} remains essentially independent of H_0, but it is *x*- and *T*-dependent because both doping and temperature change the Fe^{3+} *ac* plane anisotropy.

On the basis of the above considerations, we extracted the values of Λ for all spectra in Fig. 2, A to K, where a spectroscopic anticrossing is resolvable and plotted these values against $\sqrt{\eta_{spin}\omega_{FM}}$ in Fig. 2L. As shown in the figure, all data points fall onto a line that passes through the origin. This scaling behavior for the vacuum Rabi splitting evidences that the Er^{3+} spins are cooperatively coupled to the Fe^{3+} vacuum magnon field.

To extract more quantitative information from our experimental data, we developed a microscopic theoretical model (*18*). For the Fe^{3+} subsystem, we followed the treatment of Herrmann (*23*). The Hamiltonian $\hat{H}_{Fe}$ takes into account the symmetric exchange, antisymmetric exchange, and anisotropy of the spins in the two sublattices, $\mathbf{S}_{2l-1}$ and $\mathbf{S}_{2l}$, where $l = 1,2,\ldots,N_{UC}$ is the unit-cell index (with N_{UC} being the total number of unit cells). For the Er^{3+} subsystem, we modeled the EPR associated with the $|1-\rangle \rightarrow |1+\rangle$ transition as the Larmor precession of an Er^{3+} spin $\mathbf{R}_l$ in the *l*th unit cell. The EPR Hamiltonian is $\hat{H}_{Er} = \sum_{l=1}^{N_{UC}} -\hat{\boldsymbol{\mu}}_l \cdot \mu_0 \mathbf{H}_{DC}$, where $\hat{\boldsymbol{\mu}}_l$ is the magnetic moment, expressed as the dot product of the anisotropic Landé *g*-factor and $\mathbf{R}_l$, and μ_0 is the vacuum permeability.

The Er^{3+} EPR interacts with the Fe^{3+} qFM magnon (represented by the oscillation of $\mathbf{S}_+ = \mathbf{S}_{2l-1} + \mathbf{S}_{2l}$) through both the symmetric and antisymmetric exchange interactions (*9*). The Fe^{3+}-Er^{3+} coupling Hamiltonian for $ErFeO_3$ is

$$\hat{H}_{Fe\text{-}Er} = \sum_{l=1}^{N_{UC}} \left[J_1 \hat{\mathbf{R}}_l \cdot \hat{\mathbf{S}}_{2l-1} + J_2 \hat{\mathbf{R}}_l \cdot \hat{\mathbf{S}}_{2l} + \mathbf{D}_1 \cdot \left(\hat{\mathbf{R}}_l \times \hat{\mathbf{S}}_{2l-1} \right) + \mathbf{D}_2 \cdot \left(\hat{\mathbf{R}}_l \times \hat{\mathbf{S}}_{2l} \right) \right] \quad (1)$$

where J_1 and J_2 ($\mathbf{D}_1$ and $\mathbf{D}_2$) are the symmetric (antisymmetric) exchange constants.

From the total Hamiltonian $\hat{H} = \hat{H}_{Fe} + \hat{H}_{Er} + \hat{H}_{Fe\text{-}Er}$, we derived

$$\Lambda = \frac{J}{\hbar}\sqrt{\frac{n_{spin} V_0 \omega_{FM}}{4\gamma J_{Fe}}} = \frac{J}{\hbar\sqrt{2\gamma J_{Fe}}}\sqrt{\eta_{spin}\omega_{FM}} \quad (2)$$

where $J_1 = J_2 = J$ due to symmetry arguments, γ is the gyromagnetic ratio, and J_{Fe} is the isotropic exchange constant between the Fe^{3+} spins; J_{Fe} has been determined through previous experiments (*24*); and $\hbar$ is Planck's constant *h* divided by 2π. Equation 2 reveals the characteristic cooperative scaling behavior of Λ, supporting our experimental observation shown in Fig. 2. We determined the exchange constant $J = 2.95$ meV by fitting the slope of the $\Lambda \propto \sqrt{\eta_{spin}\omega_{FM}}$ line in Fig. 2L using Eq. 2.

Our observed Dicke cooperativity in $ErFeO_3$ opens up possibilities to realize a SRPT in thermal equilibrium. A magnon SRPT in a spin-magnon interaction system is much more feasible than a photon SRPT based on an electrical-dipolar–type light-matter interaction system (*25*). It has been speculated that some magnetic phase transitions in these orthoferrite compounds (such as $ErFeO_3$) are magnon SRPTs (*26*). Our work demonstrates the key physics required to rigorously analyze these phenomena. Furthermore, another inspiration from our observation is to control condensed matter phases on the basis of boson-mediated long-range interactions. In JT and JT-like transitions, the critical temperatures can be manipulated by changing the matter-matter interaction strength through tuning the density of the pesudospins. This raises the future possibility that Dicke physics, a well-established concept in quantum optics, can provide a guideline for controlling and engineering novel entangled phase transitions of condensed matter.

REFERENCES AND NOTES

1. R. H. Dicke, *Phys. Rev.* **93**, 99–110 (1954).
2. M. Tavis, F. W. Cummings, *Phys. Rev.* **188**, 692–695 (1969).
3. K. Hepp, E. H. Lieb, *Ann. Phys.* **76**, 360–404 (1973).
4. C. Weisbuch, M. Nishioka, A. Ishikawa, Y. Arakawa, *Phys. Rev. Lett.* **69**, 3314–3317 (1992).
5. Y. Tabuchi *et al.*, *Phys. Rev. Lett.* **113**, 083603 (2014).
6. G. Günter *et al.*, *Nature* **458**, 178–181 (2009).
7. Q. Zhang *et al.*, *Nat. Phys.* **12**, 1005–1011 (2016).
8. D. Porras, P. A. Ivanov, F. Schmidt-Kaler, *Phys. Rev. Lett.* **108**, 235701 (2012).
9. T. Yamaguchi, *J. Phys. Chem. Solids* **35**, 479–500 (1974).
10. T. Lottermoser *et al.*, *Nature* **430**, 541–544 (2004).
11. N. J. Laurita *et al.*, *Phys. Rev. Lett.* **119**, 227601 (2017).
12. L. Chaix *et al.*, *Phys. Rev. Lett.* **112**, 137201 (2014).
13. S. Baierl *et al.*, *Nat. Photonics* **10**, 715–718 (2016).
14. G. R. Stewart, *Rev. Mod. Phys.* **56**, 755–787 (1984).
15. R. L. White, *J. Appl. Phys.* **40**, 1061–1069 (1969).
16. K. Yamaguchi, T. Kurihara, Y. Minami, M. Nakajima, T. Suemoto, *Phys. Rev. Lett.* **110**, 137204 (2013).
17. J. Lu *et al.*, *Phys. Rev. Lett.* **118**, 207204 (2017).
18. See supplementary materials.
19. D. L. Wood, J. P. Remeika, L. M. Holmes, E. M. Gyorgy, *J. Appl. Phys.* **40**, 1245–1246 (1969).
20. Y. Todorov *et al.*, *Phys. Rev. Lett.* **105**, 196402 (2010).
21. P. Forn-Díaz, L. Lamata, E. Rico, J. Kono, E. Solano, arXiv:1804.09275 [quant-ph] (9 May 2018).
22. K. Zhang *et al.*, *Sci. Rep.* **6**, 23648 (2016).
23. G. Herrmann, *J. Phys. Chem. Solids* **24**, 597–606 (1963).
24. N. Koshizuka, K. Hayashi, *J. Phys. Soc. Jpn.* **57**, 4418–4428 (1988).
25. J. M. Knight, Y. Aharonov, G. T. C. Hsieh, *Phys. Rev. A* **17**, 1454–1462 (1978).
26. A. M. Kadomtseva, I. B. Krynetskii, V. M. Matveev, *Sov. Phys. JETP* **52**, 732–737 (1980).

ACKNOWLEDGMENTS

We thank A. H. MacDonald, P. Lapas, and O. Gomonay for useful discussions. **Funding:** This research was primarily supported by the National Science Foundation through the Center for Dynamics and Control of Materials: an NSF MRSEC under Cooperative Agreement DMR-1720595. J.K. acknowledges support from the U.S. Army Research Office (grant W911NF-17-1-0259). M.B. was supported by the JST PRESTO program (grant JPMJPR1767); KAKENHI (grant 26287087); and the ImPACT Program of the Council for Science, Technology and Innovation (Cabinet Office, government of Japan). D.T. acknowledges financial support from the Deutsche Forschungsgemeinschaft (SFB 1242 "Non-Equilibrium Dynamics of Condensed Matter in the Time Domain," TP B08), the European Commission (EU Career Integration grant EU CIG 334324 LIGHTER), and the Max Planck Society. S.C. acknowledges support from the National Natural Science Foundation of China (11774217). G.M. acknowledges support from the National Natural Science Foundation of China (11674213 and 61735010). Z.J. acknowledges support from the National Natural Science Foundation of China (11604202), Shanghai Municipal Education Commission (Young Eastern Scholar QD2015020), Science and Technology Commission of Shanghai Municipality (Shanghai Rising-Star Program 18QA1401700), and Shanghai Educational Development Foundation (Chen Guang project 16CG45). W.R. acknowledges support from the State Key Laboratory of Solidification Processing in NWPU (SKLSP201703) and the National Natural Science Foundation of China (51672171). **Author contributions:** X.L. performed all measurements, analyzed all experimental data, and prepared the manuscript under the supervision and guidance of J.K. M.B. developed the theoretical model to explain the experimental data. N.Y., K.X., and M.X. grew, cut, and characterized the crystals used in the experiments under the guidance of S.C. Q.Z. and Y.Z. assisted X.L. with measurements and simulations. Z.J. and D.T. characterized the THz response of the samples at low magnetic fields. All authors discussed the results and commented on the manuscript. **Competing interests:** None declared. **Data and materials availability:** All data are available in the manuscript or the supplementary materials.

SUPPLEMENTARY MATERIALS

www.sciencemag.org/content/361/6404/794/suppl/DC1
Materials and Methods
Supplementary Text
Figs. S1 to S15
Table S1
References (*27*–*33*)

7 March 2018; accepted 21 June 2018
10.1126/science.aat5162

Observation of Dicke cooperativity in magnetic interactions

Xinwei Li, Motoaki Bamba, Ning Yuan, Qi Zhang, Yage Zhao, Maolin Xiang, Kai Xu, Zuanming Jin, Wei Ren, Guohong Ma, Shixun Cao, Dmitry Turchinovich and Junichiro Kono

Science **361** (6404), 794-797.
DOI: 10.1126/science.aat5162

Cooperative quantum magnetism

One of the earliest and most intensively studied problems in quantum optics is the interaction of a two-level system (an atom) with a single photon. This simple system provides a rich platform for exploring exotic light-matter interactions and the emergence of more complex phenomena such as superradiance, which is a cooperative effect that emerges when the density of atoms is increased and coupling between them is enhanced. Going beyond the light-matter system, Li *et al.* observed analogous cooperative effects for coupled magnetic systems. The results suggest that ideas in quantum optics could be carried over and used to control and predict exotic phases in condensed matter systems.

Science, this issue p. 794